

## Predictions of magnetosheath merging between IMF field lines of opposite polarity

N. C. Maynard,<sup>1</sup> B. U. Ö. Sonnerup,<sup>2</sup> G. L. Siscoe,<sup>3</sup> D. R. Weimer,<sup>1</sup> K. D. Siebert,<sup>1</sup> G. M. Erickson,<sup>3</sup> W. W. White,<sup>1</sup> J. A. Schoendorf,<sup>1</sup> D. M. Ober,<sup>1</sup> G. R. Wilson,<sup>1</sup> and M. A. Heinemann<sup>4</sup>

Received 30 January 2002; revised 22 May 2002; accepted 22 July 2002; published 19 December 2002.

[1] Magnetohydrodynamic (MHD) simulations using the Integrated Space Weather Prediction Model (ISM) show merging in the magnetosheath between interplanetary magnetic field (IMF) field lines on opposite sides of a directional discontinuity. As the discontinuity passes the bow shock and traverses the magnetosheath, the magnetic field gradients on either side become steeper, and the geometry is distorted by the nonuniform flow speed in the magnetosheath. Associated current densities are intensified. In a location isolated from the magnetopause, we use the appearance of an  $X$  magnetic field configuration, associated dissipation electric fields, and increases in plasma velocity in the exhaust direction from the  $X$  as evidence for merging in the magnetosheath. We suggest that these signatures might be observable by Polar, as it now traverses the magnetosheath near the nose or by the Cluster spacecraft when the discontinuity is tilted away from the  $YZ$  plane. Merging signatures are seen in simulations with both  $90^\circ$  and  $180^\circ$  rotations of the field across the discontinuity. Magnetosheath merging creates a hole in the directional discontinuity, allowing the magnetosphere to penetrate through the structure as the discontinuity passes downstream. Magnetosheath merging has the potential to affect ionospheric convection pattern changes, open–closed boundaries, and magnetotail dynamics. A possible association with hot flow anomalies (HFA) is also indicated. **INDEX TERMS:** 2740 Magnetospheric Physics: Magnetospheric configuration and dynamics; 2760 Magnetospheric Physics: Plasma convection; 2784 Magnetospheric Physics: Solar wind/magnetosphere interactions; 2728 Magnetospheric Physics: Magnetosheath; **KEYWORDS:** merging, reconnection, magnetosheath, magnetopause, convection, hot flow anomalies

**Citation:** Maynard, N. C., et al., Predictions of magnetosheath merging between IMF field lines of opposite polarity, *J. Geophys. Res.*, 107(A12), 1456, doi:10.1029/2002JA009289, 2002.

### 1. Introduction

[2] While using a magnetohydrodynamic (MHD) simulation with the Integrated Space Weather Prediction Model (ISM) to investigate the effects on the magnetosphere ionosphere system from a reversal in the interplanetary magnetic field (IMF)  $B_y$ , Maynard *et al.* [2001b] found indications in the simulation results of merging in the magnetosheath between IMF field lines of opposite polarity. The reversal of the  $Y$  component of the IMF was initially applied at the upstream boundary at  $40 R_E$  and had the character of a tangential discontinuity in the solar wind. As this directional discontinuity approached the magnetopause

it became compressed and distorted by the post-bow shock slowing and deflection of the velocity in the magnetosheath. Magnetic field lines traced into the magnetosheath from the dusk edge of the simulation, outside of the bow shock, turned around and returned to the dusk edge of the simulation [Maynard *et al.*, 2001b, Plates 3, 4, and 13]. This resulted in a layer of unshocked solar wind that was magnetically connected to the magnetosheath, but not to the magnetosphere. The layer was sandwiched between regions of open field lines extending out through the magnetosheath and into the solar wind from each hemisphere. In the magnetosheath this layer advected down the flank of the magnetotail.

[3] Merging in nature occurs when the frozen-in condition of the electrons and ions is broken. In our physical understanding of merging, this may be accomplished through several terms in the generalized Ohm's law: electron pressure gradients, inertial terms, or dissipation from anomalous resistivity [see Scudder, 1997, and references therein]. Only dissipation is available to accomplish merging in our MHD simulations, whether introduced through an explicit term or entering through numerical

<sup>1</sup>Mission Research Corporation, Nashua, New Hampshire, USA.

<sup>2</sup>Thayer School of Engineering, Dartmouth College, Hanover, New Hampshire, USA.

<sup>3</sup>Center for Space Physics, Boston University, Boston, Massachusetts, USA.

<sup>4</sup>Space Vehicles Directorate, Air Force Research Laboratory, Hanscom AFB, Massachusetts, USA.

dissipation. Dissipation also occurs in the simulation in locations other than where an  $X$ -type configuration is seen. Hence, its presence does not guarantee merging, while its absence excludes active merging. The purpose of this paper is to further explore the conditions under which merging in the magnetosheath occurs in our simulations. The question must be raised as to whether merging in the simulation is a valid proxy for natural processes, or an artifact of the code that has no physical meaning. This will be addressed further in the discussion, but not definitively answered. To the degree that these simulations are representative of natural processes, these results serve as a prediction of merging in the magnetosheath and could have substantial implications relative to how the IMF couples with the magnetosphere-ionosphere system. Predictions from simulations stimulate new perspectives for data analysis, but will gain eventual acceptance only through validation with measurements. An example of this was the identification of the sash by MHD simulations [White *et al.*, 1998] and its detection with measurements from multiple satellites [Maynard *et al.*, 2001a]. Observational evidence for magnetosheath merging is needed and will be the subject of a separate investigation.

[4] We present results from 5 simulations in which a directional discontinuity was created by complete or partial reversing of the IMF in the  $YZ$  plane. The results confirm that, in the simulations, merging of IMF field lines occurs in the magnetosheath. A sixth simulation is also presented in which all three components of the IMF were equal in magnitude and were reversed to illustrate effects when the discontinuity plane is tilted [e.g., Maynard *et al.*, 2000, 2001b; Weimer *et al.*, 2002].

[5] The interaction of directional discontinuities with the bow shock is complex and nonlinear. For instance a tangential discontinuity interacting with the fast shock may split into as many as 7 new discontinuities [Neubauer, 1976], including fast and slow shocks, rotational (or Alfvén) discontinuities and refraction waves. In the simple geometry of directional discontinuities simulated here, Neubauer [1975] would predict that the primary effect beyond the shock would be to change the orientation of the initial discontinuity and compress its thickness. Lin *et al.* [1996] and Lin [1997] used two-dimensional hybrid simulations to show that the impact of tilted directional discontinuities in the solar wind on the bow shock creates a transmitted directional discontinuity in the magnetosheath that is oriented differently and compressed. Slow shock structures were too weak to be detected. These result in a pressure pulse propagating through the magnetosheath with the discontinuity. Lin [1997] also found a bulge in the magnetic field at the intersection of the discontinuity with the bow shock and sunward flow. Magnetic merging was detected in the simulations at the interaction of the discontinuity and the bow shock. They associated a bulge at the junction of the directional discontinuity with the bow shock in the simulation with hot flow anomalies (HFA). In their simulation the magnetopause was a fixed boundary.

[6] HFAs, first recognized in the particle data just outside the bow shock, have been associated with the interaction of tilted tangential discontinuities with the bow shock [Thom-

sen *et al.*, 1986, 1988; Schwartz *et al.*, 1988; Paschmann *et al.*, 1988; see also review by Schwartz *et al.*, 2000]. These structures consist of low-density, heated plasma flowing at large angles to the solar wind. A large percentage of the observations have been just outside the bow shock, but they also are seen inside the bow shock. There is a clear association with tangential discontinuities whose normals form a large angle with the Earth-Sun line [Schwartz *et al.*, 2000]. Scale sizes are a few  $R_E$  with compressed edge regions both leading and trailing the central region. Sibeck *et al.* [1999] found, for a directional discontinuity with a large tilt, that the magnetopause expanded into the directional discontinuity in the magnetosheath as the discontinuity contacted the magnetopause.

## 2. The Integrated Space Weather Prediction Model

[7] The ISM operates within a cylindrical computational domain with its origin at the center of the Earth and extending 40  $R_E$  sunward, 300  $R_E$  antisunward, and 60  $R_E$  radially from the Earth-Sun line. The domain has an interior spherical boundary at the approximate bottom of the E layer (100 km in simulations described here). ISM is based on standard MHD equations augmented with hydrodynamic equations for a collisionally coupled neutral thermosphere. As one conceptually moves inward toward the Earth, these equations transition continuously from pure MHD for plasma in the solar wind and magnetosphere to proper ionospheric/thermospheric equations at low altitudes. For purposes of the simulations discussed here, specific selections of parameters and simplifying approximations have been made. Finite difference grid resolution varies from a few hundred kilometers in the ionosphere to several  $R_E$  at the outer boundary of the computational domain. At the magnetopause, resolution ranges between 0.2 and 0.8  $R_E$ . Explicit viscosity in the plasma momentum equation has been set to zero. To approximate nonlinear aspects of magnetic reconnection within the context of a finite difference grid, the coefficient for explicit resistivity  $\eta$  in the ISM Ohm's law equation is zero when current density perpendicular to  $B$  is less than  $3.16 \times 10^{-3} \text{ A m}^{-2}$  and is  $2 \times 10^{10} \text{ m}^2 \text{ s}^{-1}$  in regions with perpendicular current density above this threshold. In practice, this choice of  $\eta$  leads to nonzero explicit resistivity primarily in the subsolar region of the dayside magnetopause, and in the plasma sheet on the nightside. Dissipation for numerical stability is based on a form of the partial donor-cell method (PDM) developed by Hain [1987].

[8] In the discussion to follow, specific simulation results are presented. The solar wind inflow boundary conditions were based on typical values: speed = 350 km s<sup>-1</sup>, density = 5 protons cm<sup>-3</sup>; temperature = 20 eV; IMF strength = 5 nT. In the simulations the direction of the IMF was switched, creating directional discontinuities in the solar wind. To reduce the computational time for these simulations, thermospheric hydrodynamics and explicit chemistry between ionospheric and thermospheric species, which have negligible impact on the results here, have not been activated in the ISM code. Ionospheric Pedersen conductance is 6 S at the pole and varies in latitude as

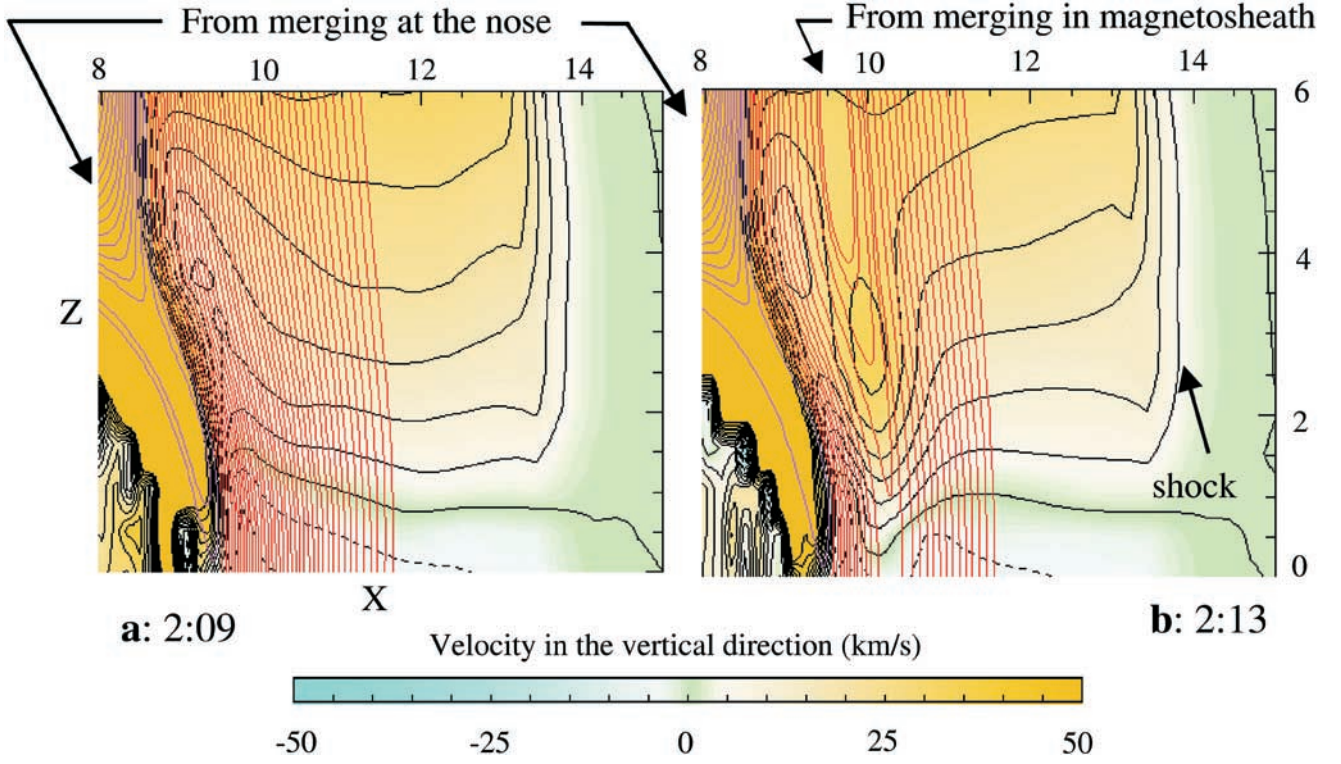


**Figure 1.** Response of the dayside magnetosheath to a directional discontinuity in the solar wind in which the IMF changes from southward to northward: (a) the  $XZ$  plane before the arrival of the directional discontinuity and (b) the  $XZ$  plane during the passage through the magnetosheath of the directional discontinuity. The background and the contours represent the velocity in the  $Z$  direction. The red lines are magnetic field lines traced from  $Z = 50 R_E$  and  $Y = 0$ . The dip in the velocity contours in the magnetosheath away from the magnetopause indicates a faster velocity in the vicinity of the discontinuity.

$B^{-2}$ . It is uniform in longitude. No Hall conductance was used. The low grid resolution at the front boundary of the model spreads out the field reversal over about  $7 R_E$ . The directional change covers about 7 grid cells in the solar wind and outer magnetosheath. Just inside the bow shock, the reversal covered 8 cells or  $1.2 R_E$  in the simulation. However, because of the bow shock, the higher grid resolution there and in the magnetosheath, and the slowing of the flow as the magnetopause is approached, the reversal in  $B$  steepens in the subsolar magnetosheath. At the nose of the magnetosphere the reversal is compressed to 5 grid cells, or about  $0.7 R_E$ . Grid resolution there is  $0.15 R_E$  in the  $X$  direction.

### 3. Simulation Results

[9] To check on the generality of the observation of magnetosheath merging reported by Maynard *et al.* [2001b], several simulation runs were performed using ISM in which directional discontinuities were created and allowed to propagate to the magnetosphere. The first run started from a relatively steady state magnetosphere, achieved after 0200 hours of run time with southward IMF, at which time the IMF was abruptly reversed from southward to northward at the front boundary. Figure 1 shows the  $XZ$  plane in the magnetosheath for two condi-

tions, one before the reversal impacted the bow shock at  $t = 0209$  hours, and one while the reversal front was in the magnetosheath at  $t = 0213$  hours. In each panel colors represent vertical ( $Z$ ) velocity, with black contours spaced  $5 \text{ km s}^{-1}$  apart. In the left panel the velocity in the sheath increases evenly away from the  $x$  axis as one moves to higher  $Z$  values, as would be expected from gas dynamic or MHD flow in the sheath. Closely spaced velocity contours and a change from green to tan in color at the right of each panel locates the bow shock. The red lines are magnetic field lines traced from the upper boundary of the simulation at intervals of  $0.1 R_E$ . The field lines that have merged with the geomagnetic field as a result of a southward IMF impinging on the nose of the magnetopause are clearly seen at the left of each panel.

[10] Compared to the plot for  $t = 0209$  hours, the plot for  $t = 0213$  hours shows two clear differences. First, between  $9.3$  and  $10 R_E$  magnetic field lines form the top half of an  $X$ -type merging configuration, reversing direction and returning to the upper boundary of the simulation. The center of the  $X$  configuration (merging location) is below the equator since there was a small dipole tilt toward the Sun of  $4^\circ$ . Second, velocity contours exhibit a valley with a minimum in the center of the  $X$  configuration. This indicates that, associated with the field line changes, the velocity increased in the

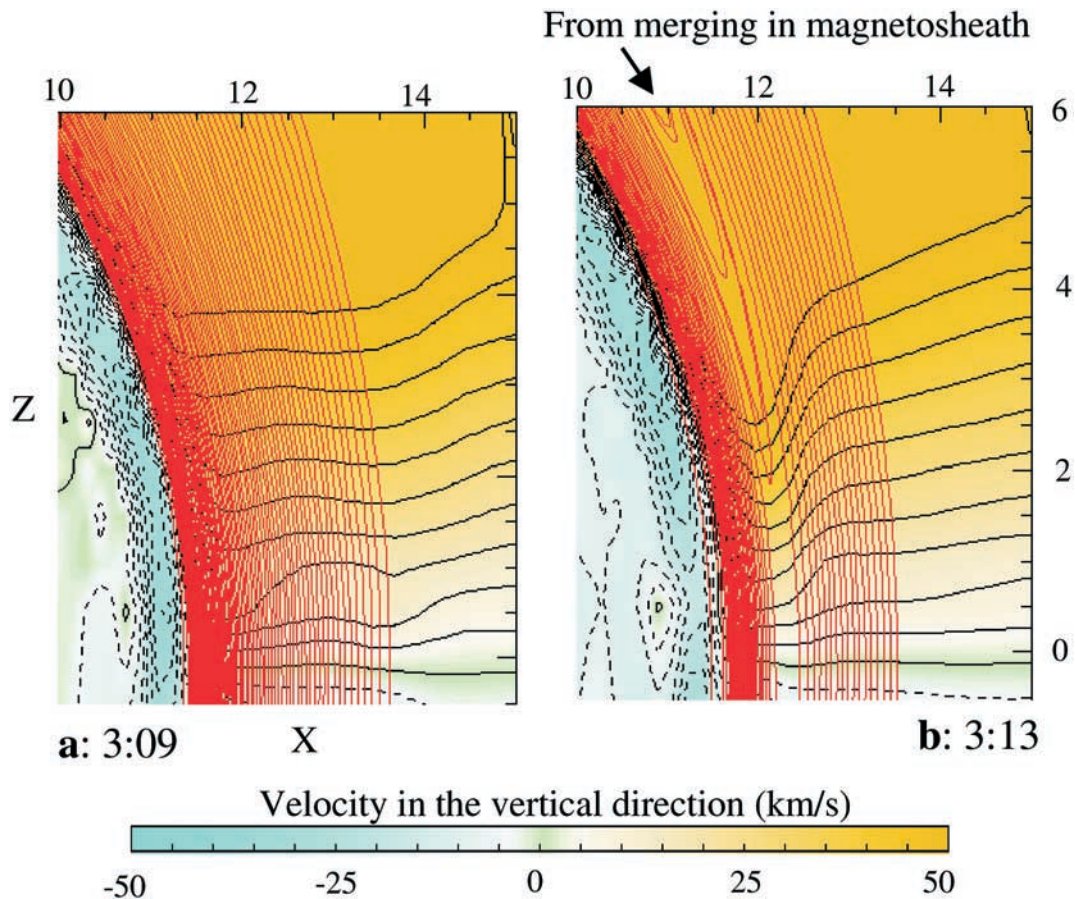


**Figure 2.** Response of the dayside magnetosheath to a directional discontinuity in the solar wind in which the IMF changes from northward to southward: (a) the  $XZ$  plane before the arrival of the directional discontinuity and (b) the  $XZ$  plane during the passage through the magnetosheath of the directional discontinuity (see caption for Figure 1).

vertical direction, away from the reconnection site, and reached a local maximum near  $3 R_E$ , as indicated by the closed, elongated contour. Note that this merging-like configuration has developed in the magnetosheath well upstream of the magnetopause. It is not part of the active merging at the nose and does not involve magnetospheric field lines. It produces merging of opposite-polarity IMF lines in the vertical plane, and is analogous to the results reported by Maynard *et al.* [2001b], in which merging between oppositely directed  $B_Y$  magnetic field lines occurred.

[11] After the IMF change had advected down the magnetotail for an hour, the IMF was reversed back to southward. The result is seen in Figure 2 in the same format as Figure 1. The magnetopause, represented by the transition from blue to tan, has moved out, as expected for this  $B_Z$  northward condition. Also for this northward IMF orientation there is no merging at the subsolar magnetopause, and thus the magnetic field intensity increases near the nose as indicated by the increase in density in the red field lines. There is a corresponding decrease in the plasma density in this depletion region (not shown), as predicted by Zwan and Wolf [1976] and seen in MHD simulations by Wu [1992], Lyon [1994], and Denton and Lyon [1996] and in ISM by

Siscoe *et al.* [2002a]. The bow shock is slightly to the right of the displayed region.

[12] The merging region at the polarity reversal seen in Figure 2b is narrower than the south-to-north transition seen in Figure 1b. The same  $X$ -type field topology near  $X = 12 R_E$  is nonetheless clear. The dip in the velocity contours is also seen, indicating increased velocity associated with the  $X$ -like configuration, although the dip is not as deep as that in Figure 1b.

[13] Figures 1 and 2 along with the results of Maynard *et al.* [2001b] provide evidence of a magnetic field topology and allied velocity increases in the magnetosheath that are associated with merging. The merging sites are isolated from the magnetopause, and involve only IMF rooted magnetic field lines. This occurs in each of the three simulations with a  $180^\circ$  reversal ( $180^\circ \rightarrow 0^\circ$ ;  $0^\circ \rightarrow 180^\circ$ ;  $90^\circ \rightarrow -90^\circ$ ). Merging continues until the discontinuity reaches the nose. Then the two halves of the  $X$  separate exposing the nose to the new IMF direction, and interaction begins with magnetospheric field lines. The merged IMF field lines curve around the edges of the discontinuity, as the merged region propagates tailward in the magnetosheath. The region in the vicinity of the discontinuity in the unshocked solar wind has no

connection to the magnetosphere. The unconnected field lines are surrounded, as they propagate tailward in the solar wind, by field lines that connect with open field lines in the magnetosphere [e.g., Maynard *et al.*, 2001b, Figures 3, 4, and 13]. We will discuss implications of these simulation results below.

[14] To further explore merging in the magnetosheath, two other simulations were performed, each starting from steady state conditions with an IMF clock angle of  $135^\circ$ . In the first simulation the  $B_Z$  component was switched, changing the clock angle to  $45^\circ$ , while in the second simulation the  $B_Y$  component was reversed, changing the clock angle to  $-135^\circ$ . Both simulations of directional discontinuities represent clock angle changes of  $90^\circ$ . Clear rotations of the magnetic field at the discontinuity, crossing the discontinuity from one side to the other, are seen in field line traces started at points on the  $x$  axis. However, it was harder to visualize the three-dimensional processes by planar plots of traced field lines.

[15] In the ISM MHD simulation, merging occurs as a result of dissipation. The electric field at each point, which is used to advance  $\mathbf{B}$ , is the sum of the dissipation electric field and the convective electric field (the source of the dissipation electric fields is discussed in section 2). The dissipation electric field can be found by subtracting the convective electric field from the total electric field at each location. *Siscoe et al.* [2002b] used the dissipation electric field as an indicator of where magnetic flux was being annihilated or merging was taking place in the simulation. For each of the five simulation results taken at a time before the directional discontinuity has contacted the magnetopause, Figure 3 displays the dissipation electric field component that is normal to the plane containing the  $X$ -type topology (the other two dissipation electric field components were near zero). This component lies in the plane of the discontinuity, as expected for merging. For the case in Figure 3a (see also Figure 1), the dissipation electric field at the center of the  $X$  is  $0.2 \text{ mV m}^{-1}$  in the  $Y$  direction and  $\mathbf{J} \cdot \mathbf{E}$  is positive. The vectors overlaid on the plots are difference velocity vectors, calculated by subtracting the velocity vectors of the undisturbed magnetosheath, before the directional discontinuity enters, from those at the time of the plot. Figures 3a and 3b correspond to the south-to-north and north-to-south rotations shown in Figures 1 and 2. Figure 3c shows the  $XY$  plane for the reversal in  $B_Y$  [Maynard *et al.*, 2001b]. Figures 3d and 3e depict the dissipation for the two cases of  $90^\circ$  direction change. Dissipation electric fields are seen in all cases at the bow shock and at the directional discontinuity. They are also seen at the magnetopause in all cases except for the northward to southward reversal, where the magnetopause merging is above the cusp at the time shown. The dissipation electric field at the directional discontinuity is as large as, or larger than, that in the bow shock. It is exceeded only by that at the magnetopause for  $B_Z$  southward cases. We caution that the presence of the dissipation field is a necessary, but not in itself a sufficient, condition for merging. It highlights where merging may be occurring in the simulation.

[16] The orange ovals emphasize outflow regions where the difference velocity peaks. In all cases the velocity

difference vectors within the directional discontinuity indicate increased flow away from the subsolar region. The velocity differences are primarily in the plane of the  $X$  and in the “exhaust” directions. There is no velocity enhancement in the direction perpendicular to the  $X$ -type merging plane. Velocity differences equal to or exceeding  $10 \text{ km s}^{-1}$  in Figure 3 (black vectors) are seen in all cases except 135:45, where values just under  $10 \text{ km s}^{-1}$  are indicated. These velocity increases are only a fraction of those expected to result from reconnection in the real system. This behavior is a direct consequence of the wide grid spacing in the simulated magnetosheath. Outside the discontinuity regions the difference vectors are generally small. In general the magnitude of the dissipation electric field increases as the directional discontinuity approaches the magnetopause and is compressed.

[17] A sixth simulation was performed starting with equal 3 nT IMF components with negative  $B_X$  and  $B_Z$  and positive  $B_Y$ . All three polarities were then reversed to create a tilted directional discontinuity. Figure 4 shows the progression of the directional discontinuity through the magnetosheath. In Figure 4 the discontinuity surface is illustrated as the location where the log of  $B$  equals 0.5. A surface on either side of the center of the reversal is defined in this way and shown by the blue contours in Figure 4a just as it is contacting the bow shock. Note that the right (sunward) surface is planar, while the left (earthward) surface is just beginning to be distorted by contact with the bow shock. The equatorial plane is colored by the log of  $B$ . The bow shock is seen by the transition from dark to light green, and the magnetosphere is identifiable by the red region. In between the two blue surfaces the black color indicates very low magnetic field. The slowing of the plasma velocity by the shock begins the compression of the directional discontinuity. The evolution of the discontinuity plane is presented every 3 min in Figures 4b–4e. The discontinuity narrows and is stretched and distorted as it progresses through the magnetosheath. At later times, the discontinuity continues to be distorted in Figures 4d and 4e, and a hole in the discontinuity surface is created in the subsolar region by the magnetosheath merging. To emphasize the size of the hole, Figures 4f and 4g show the surfaces in Figures 4d and 4e without the equatorial plane. Note that the discontinuity is totally draped over the magnetopause in Figures 4e and 4g with surface normals in the magnetosheath in significantly different directions from the normal to the plane in the solar wind. Had we shown the extension of the plane into the unshocked solar wind it would have the original orientation. The hole grows until the magnetopause totally penetrates the discontinuity. The discontinuity is a region with no connectivity to the magnetosphere as it propagates downtail in the magnetosheath [Maynard *et al.*, 2002].

[18] The directional discontinuity in Figure 4 is different from those of the other simulations in that a small magnetic field component normal to the discontinuity is introduced at the upstream boundary as the tilted plane enters the simulation. This normal component is shown in Figure 5a to have the same sense at all points along the discontinuity. The yellow field line traces were started near the center of the discontinuity at various  $Y$  locations.

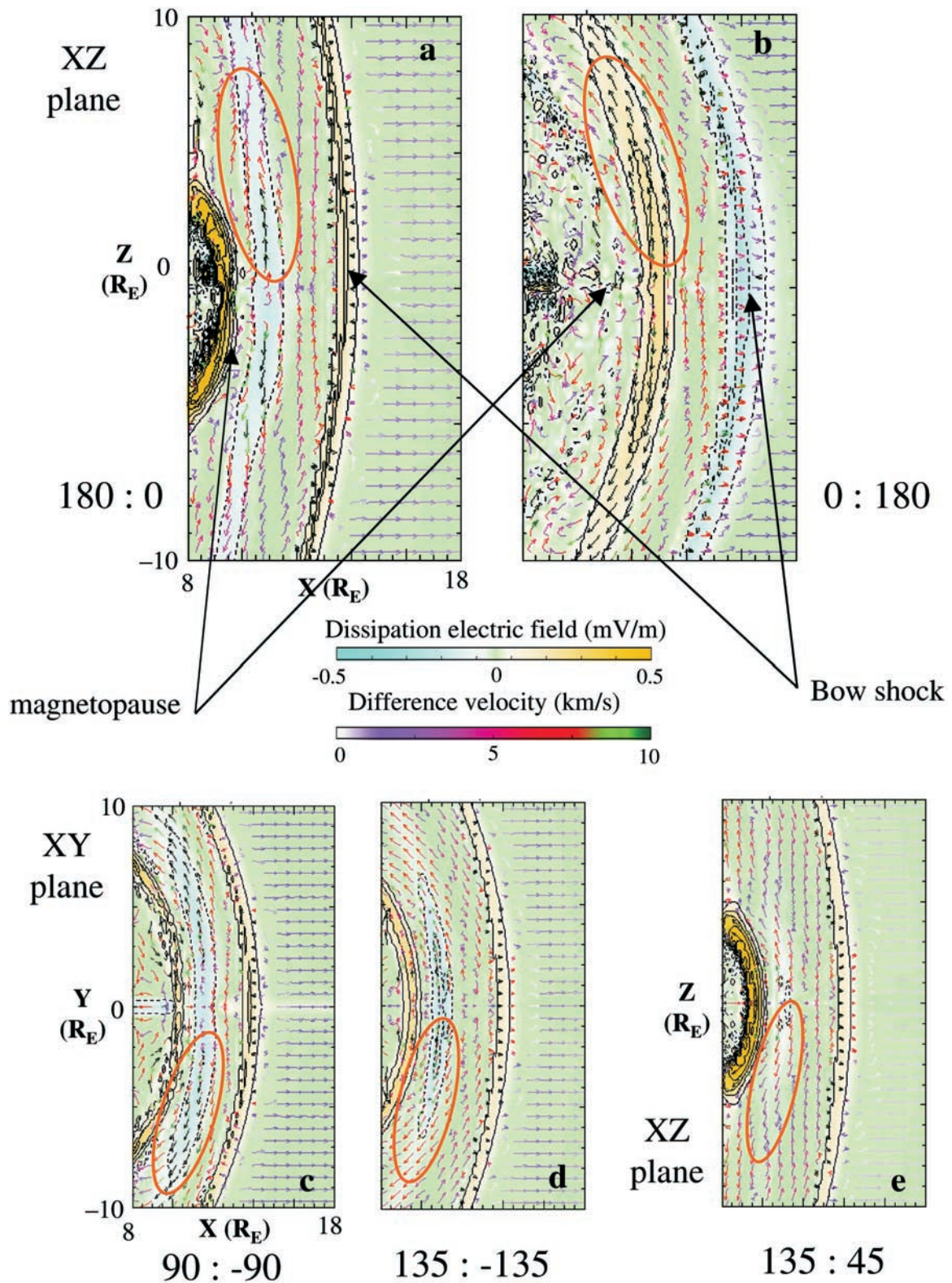


**Figure 3.** Dissipation electric fields and difference velocity vectors resulting from the passage of 5 directional discontinuities through the magnetosheath. The difference velocity vectors are from the vector subtraction of the velocity in the magnetosheath at the same point prior to the disturbance crossing the bow shock from the values at that time. The dissipation electric field is determined by subtracting the convective electric field from the total electric field at each location. Each plane is colored by the magnitude of the component of the dissipation electric field perpendicular to the plane of the directional discontinuity. The other components are near zero. The orange oval highlights the areas of maximum velocity differences in each panel.

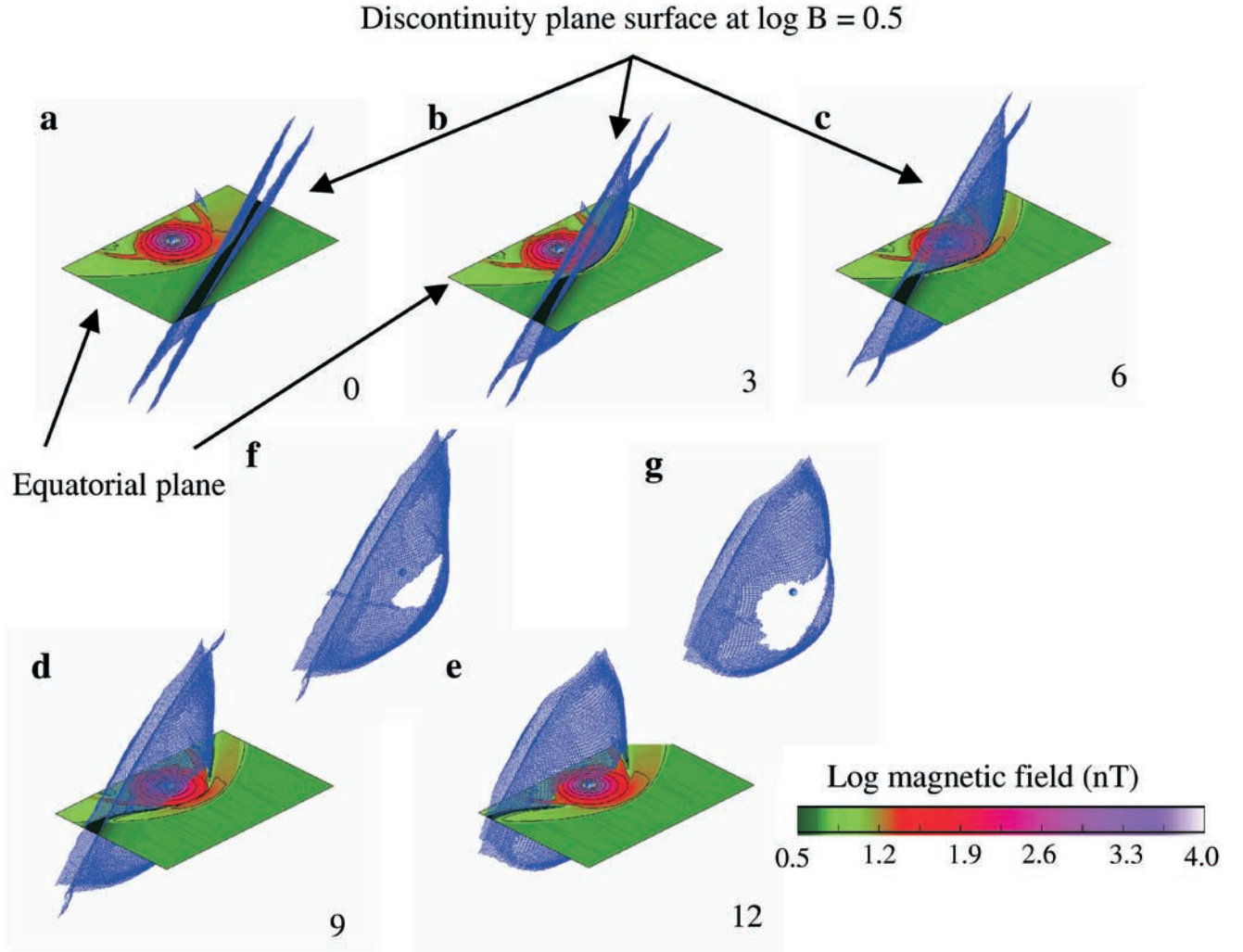


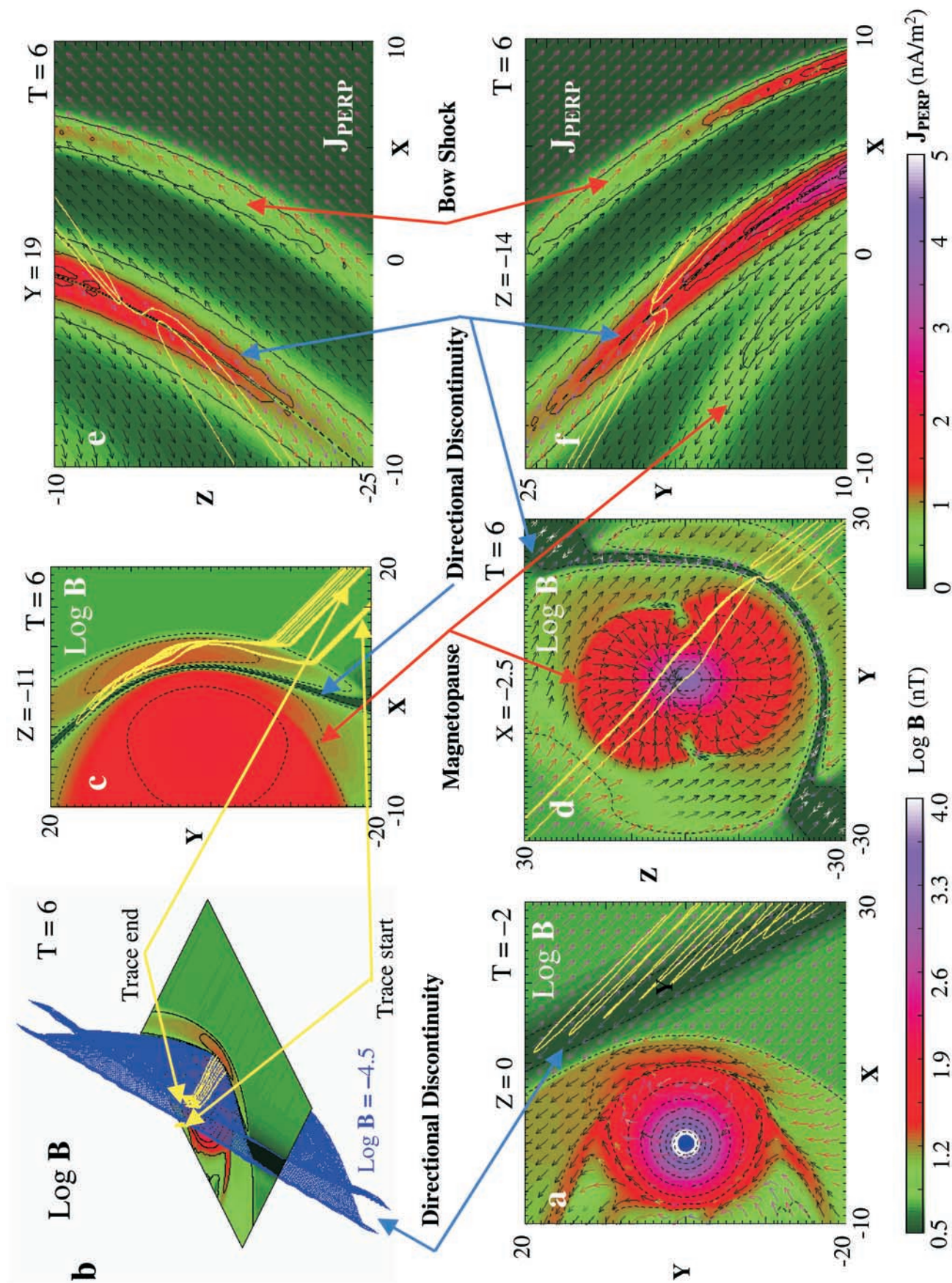
**Figure 4.** Propagation of a tilted directional discontinuity through the magnetosheath. (a)–(e) The surfaces on either side of the center of the directional discontinuity on which  $\log |B| = 0.5$  versus time. The time labeled in the lower right-hand corner is the difference between the first and the subsequent plots. The equatorial plane is colored with the magnitude of the log of  $B$ . Note in (d) and (e) that a hole in the discontinuity surface is created by magnetosheath merging, which grows and allows the magnetopause to protrude through the discontinuity surface. The hole is more clearly seen as the white regions in (f) and (g), in which the surfaces shown in (d) and (e), respectively, are repeated without the intervening plane.

In Figures 5b and 5c the yellow magnetic field lines, traced from  $-Y, +Z$  locations on the downstream side of the discontinuity, turn in the discontinuity region in the magnetosheath and return to the solar wind on the opposite side of the discontinuity. The plane in Figure 5c is at  $Z = -11 R_E$ , near where the field lines that extend the farthest turn in the discontinuity. The curvature and spacing of the projected magnetic field traces illustrate the compression of the discontinuity in the magnetosheath. An  $X$  configuration requires finding field lines that start and return to the solar wind on the dusk side. Figures 5d–5f illustrate field lines that return to both dawn and dusk from a merging site in the draped discontinuity on the dusk flank near  $X = -2.5$ ,  $Y = 19$ , and  $Z = -14$ . The three field lines that return to the dusk side in Figure 5d show that the merging region extends

along the draped discontinuity. The traces in Figures 5e and 5f are overlaid over the magnitude of the current perpendicular to  $B$ . The perpendicular current is strong in the vicinity of the  $X$ , increases toward the subsolar region within the discontinuity, and is larger than that in the nearby bow shock.

[19] Merging actually starts on the flank soon after the discontinuity crosses the bow shock. Field line traces indicate that the  $X$ -type configuration has been established in the magnetosheath within 2 min after initial contact of the discontinuity with the bow shock on the flank.

[20] As the discontinuity approaches the nose of the magnetosphere and is compressed, the perpendicular current intensifies. Figures 6a–6f show that progression in the  $Z = -14 R_E$  plane, containing the location of the merging site shown by Figures 5d–5f. The currents in the dis-



continuity are larger than those in the bow shock and approach those of the magnetopause. The currents are most intense near the nose. Figures 7g–7i show field line traces that were started in the low field region of the discontinuity near  $Y = 5$  and  $Z = 5 R_E$ . In this region at  $t = 6$  the field line traces no longer directly turn back, but tend to wander in the high-current, low magnetic field region until finding nearby field lines that return to the dawn side of the discontinuity. In some cases they wander toward dusk. It is not easy to find paired field lines in the simulation that return back to dusk to complete the merging  $X$ , as in Figures 5d–5f. Because of the normal field component in this directional discontinuity, merging near the nose from the thinning and intensifying of the current sheet would create an “O” shaped island and annihilate flux in the simulation. As a result, field line traces could wander.

[21] In summary, the chronology of events begins as the directional discontinuity impacts the bow shock. The discontinuity becomes sharper and distorts as it enters the magnetosheath. The curvature of the discontinuity surface also increases as velocity of the discontinuity in the magnetosheath is reduced while its velocity remains steady in the unshocked solar wind. Consequently the current density in the layer intensifies. Evidence of magnetosheath merging between field lines on opposite sides of the directional discontinuity is observed in simulation outputs. Signatures that indicate merging are the  $X$ -type field line configuration, the increase in velocity in the outflow region and increases in the dissipation electric field. These signatures are seen for  $90^\circ$  as well as  $180^\circ$  rotations of the field across the discontinuity. The increased current density and magnetic field line topology associated with merging occurs for tilted directional discontinuities. Magnetosheath merging starts within minutes of the initial contact of the discontinuity with the bow shock. As a result of magnetosheath merging, a hole is created in the discontinuity plane, through which the magnetopause penetrates. The directional discontinuity continues to propagate tailward without connection with the magnetosphere.

#### 4. Discussion

[22] As a directional discontinuity approaches the bow shock and magnetopause, it must be distorted in the magnetosheath from its original orientation, since the degree of slowing will be different at different  $Y$  and  $Z$

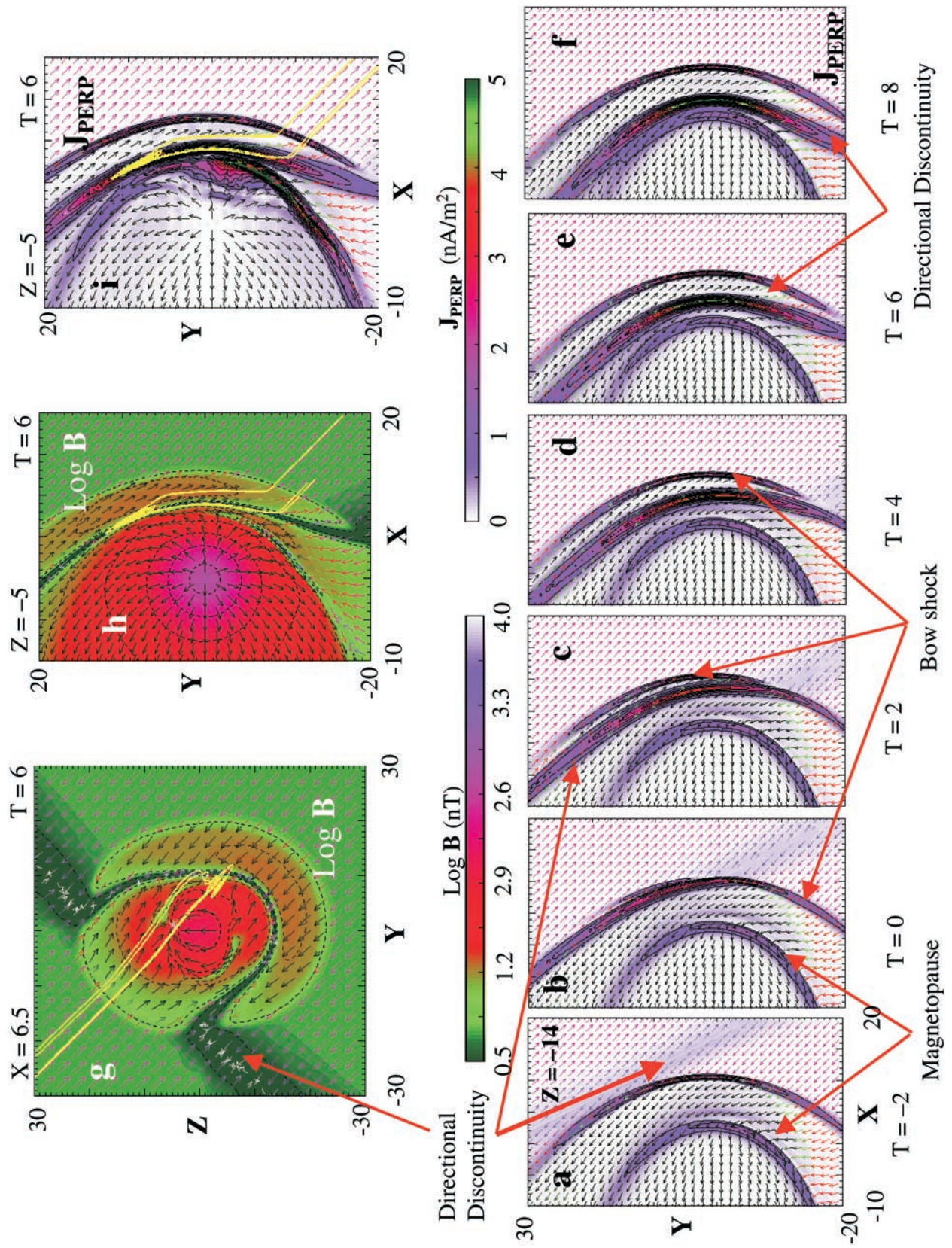
locations. The interaction of a directional discontinuity with the bow shock in the general case is nonlinear and produces multiple shocks and discontinuities [Neubauer, 1975, 1976], although for planar rotations, the primary effect on the directional discontinuity at the shock is an orientation change and compression in the transmitted discontinuity. In two-dimensional hybrid simulations Lin [1997] found the change in direction and compression of the transmitted directional discontinuity and suggested that the interaction of a tangential discontinuity with the bow shock may produce magnetic reconnection at the intersection. Resolution precluded observation of any generated slow shocks in the Lin simulation, as is the case here.

[23] The magnetopause must penetrate through this distorted structure while the undistorted part continues to be advected downstream in the unshocked solar wind. In one view, the process of penetration might be accomplished by continuous merging with magnetospheric field lines. The directional discontinuity would then become coupled to the ionosphere and remain coupled until reconnection severed that tie somewhere down the magnetotail. In simulations this is not the case. Magnetosheath merging prevents connection of the directional discontinuity to the ionosphere and opens a hole through which the magnetosphere can pass (see Figure 4). The simulations show that the field lines on each side of the directional discontinuity remain coupled and tied only to the solar wind as they propagate back through the magnetosheath [Maynard *et al.*, 2002].

[24] Merging in a MHD simulation is accomplished through dissipation. In the simulations presented in this paper the current threshold for inserting dissipation through explicit resistivity is exceeded in the current sheet of the directional discontinuity as it transitions the magnetosheath. For the northward to southward switch, it was possible to turn off the explicit dissipation. However, the code increased PDM dissipation at the discontinuity, as it steepened, and the same merging signatures were observed. The MHD solution to the applied boundary conditions requires merging in the magnetosheath, and the dissipation is introduced automatically if not present explicitly.

[25] Magnetosheath merging is a prediction of the simulations. The question arises whether, in the real system, there is time enough for merging to develop before the discontinuity reaches the magnetopause. The Geospace Environmental Modeling (GEM) Magnetic

**Figure 5.** (opposite) (a) Magnetic field line traces started in the directional discontinuity in the equatorial plane at  $t = -2$  min. The traces have a clear field component normal to the discontinuity, which is introduced at the front boundary as the tilted discontinuity plane enters the simulation. (b) Surfaces displayed in Figure 4c overlaid with magnetic field lines (yellow) traced from the edge of the simulation, which turn in the discontinuity and return to the solar wind along the opposite side of the discontinuity. (c) These same traces overlaid on the horizontal plane at  $Z = -11$  colored with the log of the magnitude of  $B$ . The most duskward trace turns in the directional discontinuity in that plane. (d)–(f) Magnetic field line traces started in the directional discontinuity. The nearly opposing traces provide evidence of an  $X$  line configuration in the region near  $X = -2$ ,  $Y = 19$ , and  $Z = -14$ . The  $YZ$  plane is colored with the log of the magnitude of  $B$ . (e) and (f) Colored with the magnitude of the perpendicular current density, illustrating that the  $X$  is centered in the current layer associated with the directional discontinuity and well separated from the bow shock and magnetopause currents. The background vectors in (c)–(f) represent the magnetic field directions in the respective planes.



Reconnection Challenge [Birn *et al.*, 2001] showed that particle, hybrid and Hall–MHD simulations produced nearly the same results, namely that peak reconnection electric fields are obtained within 15 ion gyroperiods. Assuming protons in a 30 nT magnetic field, appropriate to magnetosheath conditions considered here, those results indicate that only 30 s are required to achieve peak reconnection electric fields. According to Galeev [1981, equation (59)], the growth time for the electron tearing mode is 6 s, assuming  $B = 30$  nT,  $T_i = 1$  keV,  $T_e = 100$  eV, and a tearing wavelength of twice the assumed 100 km layer width. With a 200 km layer, the growth time would be 35 s. The transit time of the directional discontinuity from the bow shock to the nose of the magnetosphere is of the order of 4 min for the 350 km  $s^{-1}$  solar wind velocity used in the simulations, which is 7–40 times the above growth times. In the solar wind the same calculation for  $B = 10$  nT,  $T_e \approx T_i = 10$  eV, and a 1300 km average discontinuity width [Burlaga *et al.*, 1977] yields a growth time of about 20 hours. The transit time from the Sun is a smaller multiple of this growth time.

[26] In the simulations merging does not occur in the solar wind at these directional discontinuities. In over 30  $R_E$  of propagation through the interplanetary medium, no indications of merging were seen in the first 5 simulations. We conclude that with no Earth or magnetosphere being present, the directional discontinuity would in each case continue to propagate to the back of the simulation with no merging, which is consistent with the longer growth time calculated above.

[27] The question still remains whether, and to what extent, the magnetosheath merging effects seen in the simulation represent reality. Effects of merging have recently been detected in the solar wind during magnetic cloud events [Farrugia *et al.*, 2001]. We are unaware of any experimental detection of magnetosheath merging. Such an observation is needed to validate our prediction.

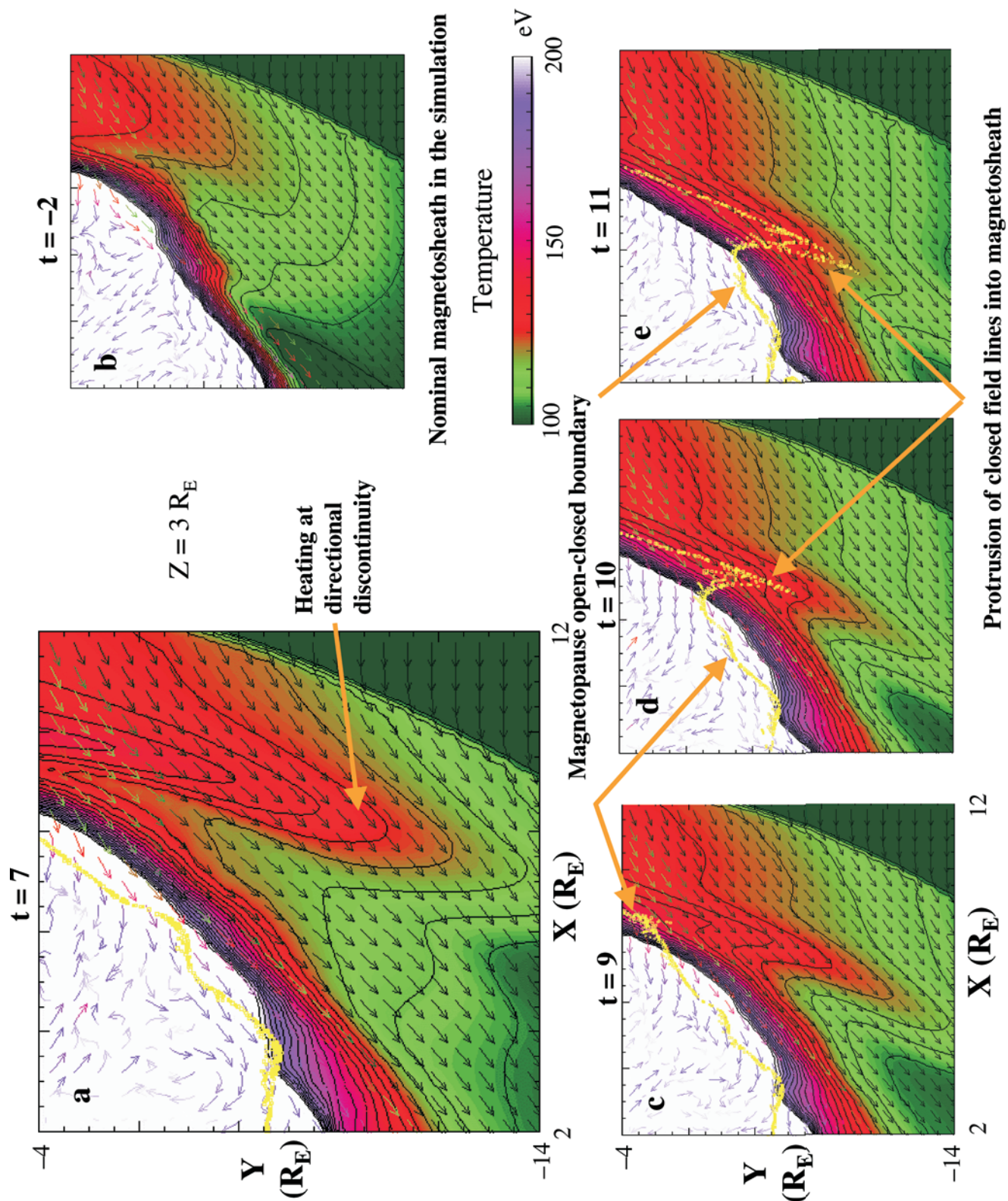
[28] The current ISTP satellite constellation presents an opportunity to look for evidence of magnetosheath merging in the data. The apogee of the Polar spacecraft is now near the equatorial plane. During March and April 2001, it spent long periods near the magnetopause and, in fact, in the magnetosheath during magnetic activity. This provides an opportunity to watch effects as directional discontinuities pass. Multisatellite constellations like Cluster have a better chance to separate spatial from temporal effects and be more definitive in the detection. Rotations in the magnetic field, localized currents and increases in the velocities in the exhaust plane are potential signatures. Scudder *et al.* [1999] have successfully performed Walén

tests on rotational discontinuities with only a partial passage through the discontinuity. This technique is useful where the satellite may be passing along rather than through the discontinuity. The phase plane of variations in the solar wind electric field, including directional discontinuities, can be tilted [e.g., Maynard *et al.*, 2000, 2001b; Weimer *et al.*, 2002], which means that it first impacts the bow shock away from the equatorial plane and may be centered at high latitudes in the magnetosheath. This potentially brings the merging region close to the Cluster orbit, making its detection more probable. The fact that effects are seen for less than 180° rotations (Figures 3d and 3e) indicates that magnetosheath merging may happen often. In the natural environment magnetosheath merging, or the difference between a nonreconnecting TD and a reconnecting discontinuity, should be detectable though several of the following properties: normal  $B$ , tangential  $E$ , positive  $E \cdot J$ , accelerated particles, parallel Poynting flux from Alfvén waves, or a successful Walén test. The satellite location relative to the nominal separator influences which test may be the most definitive.

[29] Magnetosheath merging has implications for magnetospheric phenomena. Maynard *et al.* [2001b] observed that during the  $B_Y$  polarity switch, magnetosheath merging created an interval in the IMF flowing tailward that did not connect to the open magnetosphere. As the merging site shifted from dusk to dawn in the Northern Hemisphere, the open field lines traced from the near the open–closed boundary in the ionosphere into the mantle disappeared for several minutes. Because of the reversal in  $B_x$ , azimuthal flow in the cusp must reverse. The temporary gap in the merging rate, which was caused by magnetosheath merging at the directional discontinuity, helped to implement this change. Associated with this merging interruption was a low magnetic field region around the directional discontinuity that was connected only to the IMF in the unshocked solar wind. With time this structure propagated down the tail in the magnetosheath. Maynard *et al.* [2002] combined these results with observations from Polar and ground based measurements. They found that as the directional discontinuity propagated down the flank, the low magnetic field region of the discontinuity became connected to the plasma sheet. Through the interchange instability [Kan and Burke, 1985] this high-density/low magnetic field region may provide a mechanism for short-lived Sun-aligned arcs protruding into the polar cap at the nightside open–closed boundary.

[30] Properties of HFAs [Thomsen *et al.*, 1986, 1988] have been reviewed by Schwartz *et al.* [2000]. These structures consist of low-density, heated plasma flowing at

**Figure 6.** (opposite) (a)–(f) The progression of the directional discontinuity through the magnetosheath, showing the narrowing and intensification of the currents associated with the discontinuity region from before it reached the bow shock (a) to its proximity to the magnetopause in (e) and (f). The background color depicts the magnitude of the perpendicular current. (g)–(i) Magnetic field line traces (yellow) that turn and wander in the high current region in the directional discontinuity in front of the nose of the magnetopause before returning to the dawnside solar wind. In (g) and (h), the nearly black region locates the directional discontinuity in each plane colored with the log of the magnitude of  $B$ . The color in (i) depicts the perpendicular current increase at the discontinuity and its relation to the traced field lines. The background vectors show the direction of the magnetic field in the respective planes.



large angles to the solar wind, primarily observed just outside the bow shock, but also seen inside the bow shock. Scale sizes are of a few  $R_E$  with compressed edge regions both leading and trailing the central region. The field in the center is often noisy and may be depressed or enhanced. They have been associated with the interaction of directional discontinuities or interplanetary current sheets with the bow shock. The normal to the directional discontinuity generally makes a large angle with the bow shock normal and also with the Earth–Sun line. The change in  $B$  is such that the resultant electric field from the flow in the solar wind points inward. While observations of HFAs are relatively few, *Schwartz et al.* [2000] argue that HFAs should occur at a rate of about 3 per day. To observe them, a spacecraft must be at the right place at the right time. When orbital and local time considerations are included, the 20 events observed by the AMPTE spacecraft is consistent with that rate.

[31] Recently *Sibeck et al.* [1999] observed that, as a directional discontinuity and associated HFA was encountered and subsequently moved back along the magnetopause, the latter expanded briefly into the discontinuity region. This event was observed by multiple spacecraft, and the bulge in the magnetosphere was seen to propagate tailward. Prior to the change at the directional discontinuity, the IMF was dominated by  $B_X$ . The tilt of the normal of the discontinuity plane from the Earth–Sun line was about  $60^\circ$ .

[32] The simulation of Figure 4 can be used to test the behavior of the magnetopause when a tilted directional discontinuity passes through the magnetosheath. The electric field of the directional discontinuity in Figure 4 is directed inward, consistent with conditions, given by *Schwartz et al.* [2000], for forming a HFA. The normal to the discontinuity forms an angle of about  $35^\circ$  to the  $x$  axis, which is less than typical for HFAs to develop and less than the event reported by *Sibeck et al.* [1999]. Figure 7 displays the temperature in the magnetosheath, velocity vectors and the locus of the last closed magnetic field line (yellow trace) in the  $XY$  plane at  $Z = 3 R_E$ . Figure 7a shows the temperature 7 min after the original contact with the bow shock. Figure 7b shows the nominal temperature distribution in the simulation prior to the passage of the directional discontinuity. Temperature is defined as the plasma pressure divided by the number density. Note the finger of heated ions in Figure 7a extending along the directional discontinuity. Between 9 and 11 min after first contact (Figures 7c–7e) the region of magnetospheric closed field lines extends out into the heated region of the directional discontinuity. The length of this extension along the discontinuity is between 4 and

5  $R_E$ . It begins as the directional discontinuity contacts the magnetopause. At subsequent times it advects back along the flank. The protrusion is qualitatively similar to that seen by *Sibeck et al.* [1999]. Because our directional discontinuity is tilted less than in the *Sibeck et al.* event, the interaction is delayed until the discontinuity is partially draped around the magnetopause. The protrusion lies outside the original open–closed boundary by several  $R_E$ , and the bulge moves tailward in the magnetosheath. Had the tilt of the discontinuity plane been greater, similar to the observations, the extension of the closed field line region into the magnetosheath would have been more toward the bow shock as they observed. We suggest that the outward protrusion of closed magnetic field lines into the discontinuity region is related to the interaction of the directional discontinuity with the magnetopause. Previous magnetosheath merging provides a temporary halt to merging of the IMF to magnetospheric field lines when the directional discontinuity contacts the magnetopause. The outward pressure of the closed field line region apparently pushes the open–closed boundary into the directional discontinuity. Prior to the directional discontinuity contacting the magnetopause, magnetosheath merging could be expected to locally accelerate the magnetosheath population.

## 5. Summary

[33] The ISM simulations predict that merging between IMF field lines on opposite sides of a directional discontinuity will occur in the magnetosheath. The chronology of events begins as the directional discontinuity impacts the bow shock. The discontinuity becomes sharper and distorted as it enters the magnetosheath. The curvature of the discontinuity surface increases as the velocity of the discontinuity in the magnetosheath is reduced while it remains steady in the unshocked solar wind. Associated currents are intensified in the distorted region. Increases in velocity in the exhaust direction, an  $X$  magnetic field configuration and dissipation electric fields isolated from the magnetopause are taken as evidence for magnetosheath merging. Effects are seen in simulations with both  $90^\circ$  and  $180^\circ$  rotations. Magnetosheath merging needs verification with observations. We suggest that these predictions should be observable with the Cluster spacecraft when the discontinuity is tilted away from the  $YZ$  plane and by Polar now that its apogee is near the equator. Magnetosheath merging can be expected to affect ionospheric convection pattern changes, open–closed boundaries, and magnetotail dynamics. The simulations indicate a protrusion of the magnetopause into the discontinuity region as it

**Figure 7.** (opposite) Results from a simulation including  $B_X$ . (a) The  $XY$  plane, colored with the temperature, at  $Z = 3 R_E$  7 min after initial contact of the directional discontinuity with the bow shock. The vectors show the velocity, while the yellow trace indicates the open–closed magnetic field line boundary. The nominal simulation behavior of the temperature in the magnetosheath, as seen at 2 min before first contact, is shown in (b). (c)–(e) The  $XY$  plane at  $Z = -3 R_E$ , colored with the temperature, is shown at  $t = 9, 10$ , and  $11$  min during the passage of the directional discontinuity. The yellow curves in each panel show the intersection of the last closed field line surface with that plane. The red tongue of increased temperature points to the location at each time of the directional discontinuity. Note the protrusion of closed field lines into the open field line region along the discontinuity, which develops quickly between 9 and 11 min.

contacts the magnetopause, comparable to one observed in association with HFAs. Merging may also be an energization source for HFAs.

[34] **Acknowledgments.** This work was supported in part by NASA grants NAG5-8135 (Sun-Earth Connections Theory Program grant) and NASW-99014. The ISM was developed under sponsorship of the Defense Threat Reduction Agency, 45045 Aviation Drive, Dulles, VA 20166-7517.

## References

- Birn, J., et al., Geospace Environment Modeling (GEM) magnetic reconnection challenge, *J. Geophys. Res.*, **106**, 3715, 2001.
- Burlaga, L. F., J. F. Lemaire, and J. M. Turner, Interplanetary current sheets at 1 AU, *J. Geophys. Res.*, **82**, 3191, 1977.
- Denton, R. E., and J. G. Lyon, Density depletion in an anisotropic magnetosheath, *Geophys. Res. Lett.*, **23**, 2891, 1996.
- Farrugia, C. J., et al., A reconnection layer associated with a magnetic cloud, *Adv. Space Res.*, **28**(5), 759–764, 2001.
- Galeev, A. A., Magnetospheric tail dynamics, in *Magnetospheric Plasma Physics*, edited by A. Nishida, pp. 143–196, D. Reidel, Norwell, Mass., 1981.
- Hain, K., The partial donor cell method, *J. Comput. Phys.*, **73**, 131, 1987.
- Kan, J. R., and W. J. Burke, A theoretical model of polar cap auroral arcs, *J. Geophys. Res.*, **90**, 4171, 1985.
- Lin, Y., Generation of anomalous flows near the bow shock by the interaction of interplanetary discontinuities, *J. Geophys. Res.*, **102**, 24,265, 1997.
- Lin, Y., D. W. Swift, and L. C. Lee, Simulation of pressure pulses in the bow shock and magnetosheath driven by variations in the interplanetary magnetic field orientation, *J. Geophys. Res.*, **101**, 27,251, 1996.
- Lyon, J. G., MHD simulations of the magnetosheath, *Adv. Space Res.*, **14**, 21, 1994.
- Maynard, N. C., et al., Driving dayside convection with northward IMF: Observations by a sounding rocket launched from Svalbard, *J. Geophys. Res.*, **105**, 5245, 2000.
- Maynard, N. C., G. L. Siscoe, B. U. Ö. Sonnerup, W. W. White, K. D. Siebert, D. R. Weimer, G. M. Erickson, J. A. Schoendorf, D. M. Ober, and G. R. Wilson, The response of ionospheric convection to changes in the IMF: Lessons from a MHD simulation, *J. Geophys. Res.*, **106**, 21,429, 2001a.
- Maynard, N. C., W. J. Burke, P. E. Sandholt, J. Moen, D. M. Ober, M. Lester, D. R. Weimer, and A. Egeland, Observations of simultaneous effects of merging in both hemispheres, *J. Geophys. Res.*, **106**, 24,551, 2001b.
- Maynard, N. C., et al., Responses of the open-closed field line boundary in the evening sector to IMF changes: A source mechanism for Sun-aligned arcs, *J. Geophys. Res.*, **107**, doi:10.1029/2001JA000174, in press, 2002.
- Neubauer, F. M., Nonlinear oblique interaction of interplanetary discontinuities with magnetogasdynamic shocks, *J. Geophys. Res.*, **80**, 1213, 1975.
- Neubauer, F. M., Nonlinear interaction of discontinuities in the solar wind and the origin of slow shocks, *J. Geophys. Res.*, **81**, 2248, 1976.
- Paschmann, G., G. Haerendel, N. Sckopke, E. Möbius, H. Lüher, and C. W. Carlson, Three-dimensional plasma structures with anomalous flow directions near the Earth's bow shock, *J. Geophys. Res.*, **93**, 11,279, 1988.
- Scudder, J. D., Theoretical approaches to the description of magnetic merging: The need for finite  $\beta_e$ , anisotropic, ambipolar Hall MHD, *Space Sci. Rev.*, **80**, 235, 1997.
- Scudder, J. D., P. A. Puhl-Quinn, F. S. Mozer, K. W. Ogilvie, and C. T. Russell, Generalized Walén tests through Alfvén waves and rotational discontinuities using electron flow velocities, *J. Geophys. Res.*, **104**, 19,817, 1999.
- Schwartz, S. J., R. M. Kessel, C. C. Brown, L. J. C. Woolliscroft, M. W. Dunlop, C. J. Farrugia, and D. S. Hall, Active current sheets near the Earth's bow shock, *J. Geophys. Res.*, **93**, 11,295, 1988.
- Schwartz, S. J., G. Paschmann, N. Sckopke, T. M. Bauer, M. Dunlop, A. N. Fazakerly, and M. F. Thomsen, Conditions for the formation of hot flow anomalies at Earth's bow shock, *J. Geophys. Res.*, **105**, 12,639, 2000.
- Sibeck, D. G., et al., Comprehensive study of the magnetopause response to a hot flow anomaly, *J. Geophys. Res.*, **104**, 4577, 1999.
- Siscoe, G. L., G. M. Erickson, B. U. Ö. Sonnerup, N. C. Maynard, J. A. Schoendorf, K. D. Siebert, D. R. Weimer, W. W. White, and G. R. Wilson, MHD properties of magnetosheath flow, *Planet. Space Sci.*, **50**, 2002a.
- Siscoe, G. L., G. M. Erickson, B. U. Ö. Sonnerup, N. C. Maynard, J. A. Schoendorf, K. D. Siebert, D. R. Weimer, W. W. White, and G. R. Wilson, Flow-through magnetic reconnection, *Geophys. Res. Lett.*, **29**(13), 1626, doi:10.1029/2001GL013536, 2002b.
- Thomsen, M. F., J. T. Gosling, S. A. Fuselier, S. J. Bame, and C. T. Russell, Hot, diamagnetic cavities upstream from the Earth's bow shock, *J. Geophys. Res.*, **91**, 2961, 1986.
- Thomsen, M. F., J. T. Gosling, S. J. Bame, K. B. Quest, C. T. Russell, and S. A. Fuselier, On the origin of hot diamagnetic cavities near the Earth's bow shock, *J. Geophys. Res.*, **93**, 11,311, 1988.
- Weimer, D. R., D. Ober, N. C. Maynard, W. J. Burke, M. R. Collier, D. J. McComas, N. F. Ness, and C. W. Smith, Variable time delays in the propagation of the interplanetary magnetic field, *J. Geophys. Res.*, **107**(A8), 1210, doi:10.1029/2001JA0009102, 2002.
- White, W. W., G. L. Siscoe, G. M. Erickson, Z. Kaymaz, N. C. Maynard, K. D. Siebert, B. U. Ö. Sonnerup, and D. R. Weimer, The magnetospheric Sash and cross-tail S, *Geophys. Res. Lett.*, **25**, 1605–1608, 1998.
- Wu, C. C., MHD flow past an obstacle: Large-scale flow in the magnetosheath, *Geophys. Res. Lett.*, **19**, 87, 1992.
- Zwan, B. J., and R. A. Wolf, Depletion of solar wind plasma near a planetary boundary, *Geophys. Res. Lett.*, **81**, 1636, 1976.

G. M. Erickson and G. L. Siscoe, Center for Space Physics, Boston University, 725 Commonwealth Avenue, Boston, MA 02543, USA. (gary.erickson@hanscom.af.mil; siscoe@bu.edu)

M. A. Heinemann, Air Force Research Laboratory, VSBX, 29 Randolph Road, Hanscom AFB, MA 01731-3010, USA. (michael.heinemann@hanscom.af.mil)

N. C. Maynard, D. M. Ober, J. A. Schoendorf, K. D. Siebert, D. R. Weimer, W. W. White, and G. R. Wilson, Mission Research Corporation, 589 West Hollis Street, Suite 201, Nashua, NH 03062, USA. (nmaynard@mrcnh.com; dober@mrcnh.com; jschoendorf@mrcnh.com; ksiebert@mrcnh.com; dweimer@mrcnh.com; bwhite@mrcnh.com; gwilson@mrcnh.com)

B. U. Ö. Sonnerup, Thayer School of Engineering, Dartmouth College, Hanover, NH 03755, USA. (sonnerup@dartmouth.edu)